The Pennsylvania State University

The Graduate School

Eberly College of Science

THE EFFECT OF CRYSTAL STRUCTURE ON THE MORPHOLOGY OF MARINE AEROSOL AND DESIGN OF TPD SPECTROMETER FOR UHV CHAMBER

A Thesis in

Chemistry

by

Alexander Ucci

Submitted in Partial Fulfillment
of the Requirements
for the Degree of

Master of Science

May 2014

The thesis of Alexander Ucci was reviewed and approved* by the following:

Miriam A. Freedman
Assistant Professor of Chemistry
Thesis Advisor

Nicholas Winograd
Professor of Chemistry

Thomas Mallouk
Professor of Chemistry

Jerry Y. Harrington
Associate Professor of Meteorology

Kenneth S. Feldman
Professor of Chemistry
Graduate Program Chair

*Signatures are on file in the Graduate School

ABSTRACT

Aerosol particles are ubiquitous in the atmosphere and have consequences for the climate, environment, and human health. To gain a better understanding of aerosol particles, the morphology and surface properties are investigated in two separate projects. Transmission electron microscopy (TEM) coupled with energy dispersive X-ray spectroscopy (EDS) are used to determine the structure and composition of sea salt particles, which play an important role in the marine boundary layer. In a separate project, an Ultra High Vacuum (UHV) instrument with temperature programmed desorption (TPD) capabilities is used to gain a better understanding of adsorbate-adsorbate and adsorbate-substrate interactions on atmospherically relevant substrates. To improve sensitivity to the desorption of water, a Feulner cap was designed and placed over the ionization volume of the mass spectrometer. By performing laboratory studies on the morphology and surfaces of aerosol particles, better parameters for climate models can be developed. Minimizing discrepancies between satellite retrievals and climate models will allow future changes to the climate to be predicted more accurately.

TABLE OF CONTENTS

LIST OF FIGURES

LIST OF TABLES

LIST OF ABBREVIATIONS

CCN	Cloud Condensation Nuclei
IPCC	Intergovernmental Panel on Climate Change
CTM	Chemical Transport Models
DRH	Deliquescence Relative Humidity
ERH	Efflorescence Relative Humidity
TPD	Temperature Programmed Desorption
PAH	Polycyclic Aromatic Hydrocarbon
VOC	Volatile Organic Compound
SAM	Self-Assembled Monolayer
STXM	Scanning Transmission X-ray Microscopy
NEXAFS	Near-edge X-ray Absorption Fine Structure
TEM	Transmission Electron Microscopy
EDS	Energy Dispersive X-ray Spectroscopy
SAED	Selected Area Electron Diffraction
SDS	Sodium Dodecyl Sulfate
UHV	Ultra-high Vacuum
AFM	Atomic Force Microscopy
FTIR	Fourier Transform Infrared Spectroscopy
MS	Mass Spectrometry
QMS	Quadrupole Mass Spectrometer
ASW	Amorphous Solid Water

HOPG	Highly Oriented Pyrolytic Graphite
XPS	X-ray photoelectron spectroscopy

ACKNOWLEDGEMENTS

I would first like to thank Dr. Freedman for the opportunity to work in her research group. I have had many fortunate opportunities and am grateful for her patience, guidance, and enthusiasm. I would also like to thank shared research facilities who have helped me immensely with my research projects. I would also like to acknowledge the members of the Freedman group who have provided me with guidance on my projects as well. Lastly, I would like to also give a personal thanks to my family and friends who have supported me in my time at graduate school.

Chapter 1

Introduction

1.1 Aerosol Particles

Atmospheric aerosol particles, which are ubiquitous in the atmosphere, have critical consequences for climate, environment, and health. Aerosol particles play a direct role in Earth's radiation budget by scattering and absorbing incoming solar and emitted terrestrial radiation. Reactions can also take place at the surface of aerosol particles therefore affecting concentrations of trace gases such as NO_x, O_3, and OH. Particles also have an indirect effect by having the potential to act as cloud condensation nuclei (CCN) affecting the microphysical properties of clouds. An increase in the number of aerosol particles results in both an increase in the number of droplets and decrease in droplet size in clouds. Not only does this increase the reflectivity of the cloud, but the lifetime of the cloud is extended since smaller droplets are less likely to precipitate.[1, 2] Epidemiological studies have also shown that fine particulate matter is correlated with severe health effects such as enhanced mortality, cardiovascular, and respiratory diseases.[3, 4] Despite these wide-range of effects, aerosol particles remain the most poorly understood components of the atmosphere as shown in the assessment report released by the Intergovernmental Panel on Climate Change (IPCC).[5]

1.2 Sea Salt Aerosol Particles

Sea salt aerosol particles, which largely contain NaCl, are an important particle type due to their ubiquity and their reactivity in the atmosphere. With an estimated production rate of 1,000-10,000 Tg per year, sea-salt aerosols are the largest emission by

mass.[6] These particles are hygroscopic and can potentially act as CCN in the atmosphere. The reactions of sea salt particles can also release chlorine atoms which can catalytically destroy ozone. Concentrations of reactive mercury, sulfur compounds, and other constituents in the atmosphere can be affected as well through the heterogeneous chemistry of sea salt aerosols.[7, 8, 9]

Sea salt aerosols are generated by breaking waves on ocean surfaces by a process known as bubble bursting.[10] When waves break, roughly 50% of the energy is released by entraining air in the water, which creates bubbles that rise and burst at the water surface.[11] Particles with diameters from 5 to 300 nm are released by this mechanism.[12] The release of sea salt is also dependent on wind-speed as white caps begin to appear around 3 m/s. Despite their importance and abundance in the atmosphere, sea salt aerosols are still poorly quantified. Comparing various chemical transport models (CTMs), calculated sea salt emissions have the largest inter-model differences among all types of aerosols.[13] Laboratory, coastal, and open ocean measurements are used as a basis for CTMs to determine the flux of sea salt aerosols and its dependence on wind speed. The results from these studies vary leading to a discrepancy in the determined concentration of sea salt aerosols. Many model parameterizations also assume emissions are directly proportional to whitecap coverage and a constant wind speed of roughly 3 m/s.[14] Therefore, small changes in wind speed can lead to large variations in predicted emissions of sea salt particles. Measurements near the coast can be influenced by local surf conditions therefore the measurements may not be indicative of concentrations in the open ocean.[15] The many chemical species found in seawater present additional complexities to modeling sea salt aerosol particles and their emissions into the

atmosphere. It is therefore necessary that further laboratory studies are performed on sea salt particles so the atmospheric burden of sea salt particles can be better evaluated.

While many laboratory studies use NaCl as a proxy for marine aerosol, sea water consists of a complex mixture of inorganic and organic constituents with much of the organic fraction coming from living organisms in the ocean. NaCl is the principle inorganic component of seawater with smaller amounts of cations and anions such as Mg^{2+}, Ca^{2+}, K^{+}, SO_4^{2-}, and Br^{-}. The organic components in seawater primarily consist of fatty acids such as palmitic, myristic, stearic, and lauric acid.[16] As marine organisms die, the hydrophobic cellular constituents rise to the surface of the ocean and float at the ocean water/air interface with an estimated total mass flux of about 200 Tg C/yr.[17] The organic mass fraction in marine aerosols is estimated to be 10 wt.% but could be as high as 60 wt.% in areas of the ocean with high biological activity.[18,19] As a sea salt aerosol is released, it is comprised of the many components of ocean water. Due to their ubiquity at various altitudes in the troposphere, sea salt aerosols can exist both as aqueous or solid particles.

The morphology and surface properties of sea salt aerosol particles are investigated in two separate projects. Transmission electron microscopy is used to determine the shape of laboratory proxies for sea salt aerosol particles. Individual salts are first studied and binary mixtures are then investigated to determine how composition affects overall structure. A separate project involves using a mass spectrometer in a UHV system to perform temperature programmed desorption spectroscopy (TPDS) on NaCl surfaces. The purpose of this study is to determine the energetics of water desorption from the surface.

Chapter 2

Morphology of Sea Salt Aerosols using TEM/EDS

2.1 Morphology of Sea Salt Aerosols

Sea salt particles are chemically and physically processed in the atmosphere once ejected from the ocean surface. Sea salt aerosols are hygroscopic but still undergo deliquescence and efflorescence phase changes depending on the relative humidity (Figure 1). The deliquescence relative humidity (DRH) is the point at which a particle spontaneously uptakes water. The efflorescence relative humidity (ERH) is the point at which a particle loses all of its water to form a crystal. As aerosol particles travel into the atmosphere and are exposed to drier air masses, they can exist in their effloresced form.

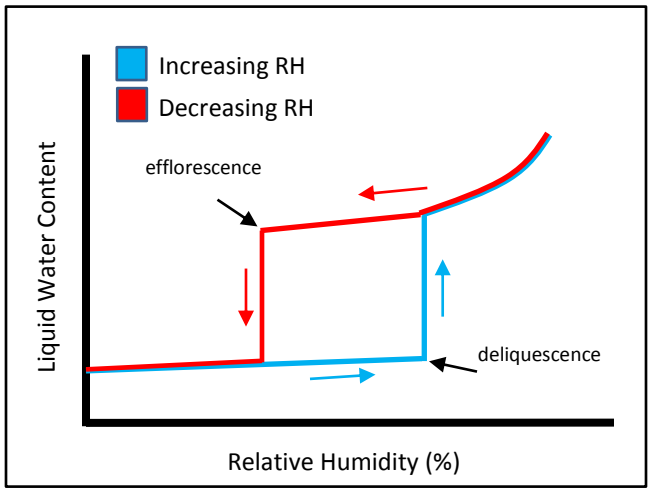

Figure 1. An example plot of deliquescence and efflorescence as a function of relative humidity.

Sea salt aerosols are a mixture of salts and we are interested how the ERH of one component in an aerosol particle will influence the structure of an internally mixed particle to obtain a better understanding of the internal structure or morphology of an aerosol particle. One study of 80-100 µm droplets containing salts relevant to seawater

demonstrated that the components crystallized sequentially at different relative humidities.[20] While there have been a number of studies on particle morphology,[21,22,23,24,25,26] the morphology of an aerosol particle remains poorly understood and no studies of particle morphology have focused on sea salt aerosols. The morphology of a particle can have many consequences for the optical properties, cloud formation, ice nucleation, and heterogeneous chemistry of the particle in the atmosphere.

2.2 Experimental

To investigate the effect of how the efflorescence of one component in a particle will affect the morphology of the internally mixed particles, we have focused on cubic salts including NaCl, NaBr, and NaI. NaCl and NaBr were investigated as they are two components of sea salt with a Cl:Br mole ratio of approximately 650:1 in seawater.[27] While NaI is not atmospherically relevant, this salt was used for its different crystal lattice spacing. These cubic salts have measured efflorescence values of 46 ± 2% (NaCl) , 22 ± 1% (NaBr) , and 10 ± 1% (NaI) using scanning transmission X-ray microscopy (STXM) and near-edge X-ray absorption fine structure (NEXAFS).[28]

Single-component systems were first analyzed to determine the initial structure of each salt. These salts were then combined to have a binary component system (i.e. NaCl and NaBr) and the morphology was investigated at varying ratios of each salt in solution. Transmission electron microscopy (TEM) is used to determine the morphology of the single salts and binary salt systems. The interaction of the sample with the electrons is used to form the image. Areas that appear dark in the image will correspond to a particle as less light is transmitted. Particles comprised of multiple components will have varying amounts of contrast which can be evidence for phase-separation in the particle.

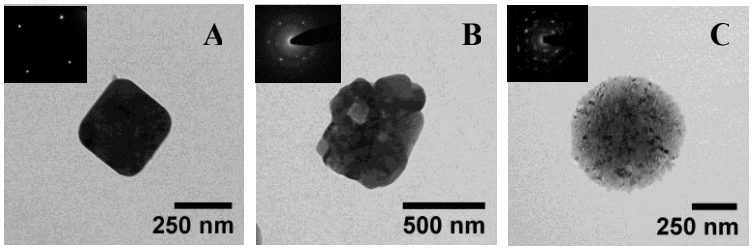

Figure 2: TEM images of (a) NaCl, (b) NaBr, and (c) NaI with the inset as the SAED patterns.

As the electrons interact with the sample, the particles can also undergo damage by the electron beam. Each compound damages differently providing qualitative information on the composition of a specific particle. Energy dispersive X-ray Spectroscopy (EDS) is used to confirm the spatially-resolved elemental composition of particles and selected area electron diffraction (SAED) is used for the examination of the crystalline structure. Particles were produced from an aqueous solution and using a constant output atomizer. They were subsequently dried using a diffusion drier and impacted onto continuous carbon coated copper grids for analysis with TEM.

TEM images of NaCl, NaBr, and NaI are shown along with the accompanying SAED patterns (Figure 2). As seen from diffraction patterns, the NaCl particles are single crystals, while NaBr and NaI are polycrystalline. The NaCl diffraction pattern consists of a single lattice whereas NaBr and NaI are composed of many different lattices superimposed on each other.

2.3 NaCl and NaBr System

When internally mixed particles containing NaCl and NaBr are imaged, we observe that the particles are phase separated as indicated by both the damaging behavior of NaCl and NaBr as well as the difference in contrast between the different components of the particle (Figure 3). As NaCl is damaged, small bubbles appear on the outer edge

of the particle and the particle becomes white in appearance from the exterior to the interior of the particle. NaBr also damages similarly but lacks the bubbles that appear on the NaCl. The shape of NaBr is affected at all concentrations with a more rod-like structure at higher concentrations of NaBr.

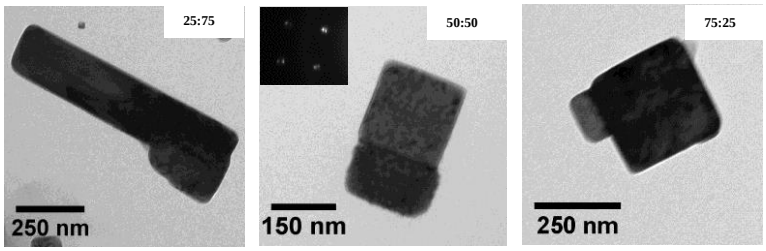

Figure 3: TEM images of binary mixtures of NaCl and NaBr. The inset of the 50:50 mixture image is the SAED pattern.

We have verified that the particles phase separate using EDS to obtain the elemental composition at specific locations on the particles (Figure 4). The particles of interest in this study are phase separated and have a significant contrast in the image allowing us to differentiate between the different components. The electron beam is focused and reduced in size to about 100 nm and used to analyze the different components of the particle. From these spectra, we observe enhancement of Cl on one side of the particle and enhancement of Br on the other side of the particle; indicating that the NaCl and NaBr have phase separated, although the phase separation may not be complete. Examining the morphology of the mixed 50:50 system, both components (Figure 3) are similar in shape to NaCl with a square or rectangular-like shape rather than more spherical like pure NaBr. SAED images indicate that both the NaBr and NaCl components of the particle are single crystals. The d-spacings observed in the diffraction pattern are determined using the equation,

$$Rd = \lambda L \qquad \text{Equation 1}$$

where R is the measured distance between the two diffraction spots and L is a constant related to the distance between the camera to the sample.[29]

The values we obtained for the lattice spacings of NaCl and NaBr were 5.601 and 5.948 Å, respectively. These values correlate well with the accepted lattice spacings of NaCl and NaBr which are 5.627 and 5.95 Å, respectively.[30]

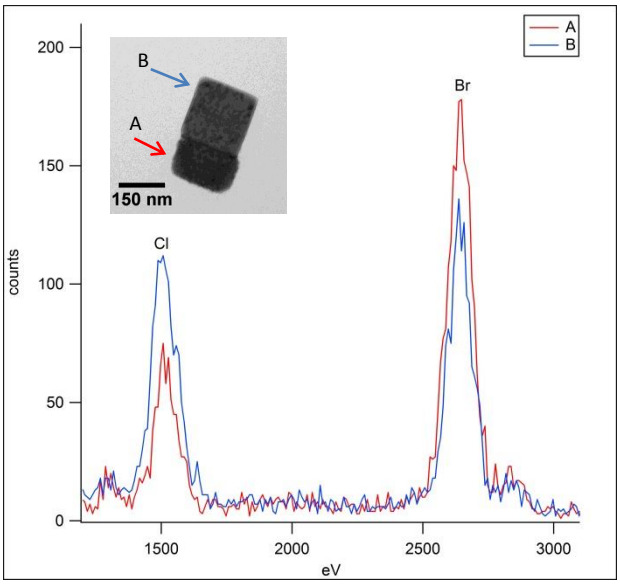

Figure 4. EDS spectrum of a NaCl:NaBr 50:50 particle. The side of the particle, A, is enhanced with Br while the other side of the particle, B, is enhanced with Cl.

The results we obtained suggest that the crystallization of NaCl provides a template for NaBr crystallization. The ERH of NaCl is 46% RH and the ERH of NaBr is 22% RH. Therefore, as the aqueous aerosol is dried, NaCl crystallizes prior to NaBr. As NaCl dries, it undergoes homogenous nucleation to form a single crystal as shown in Fig 2a. However, NaBr is likely to form a nucleus in a heterogeneous process due to the

presence of NaCl. A heterogeneous nucleation process is favored as the NaCl provides a surface for the NaBr to nucleate; which lowers the barrier for this process to occur. NaCl influences the structure of NaBr at all concentrations studied (10-90% NaCl) allowing it to form a single-crystal. At the lowest concentrations of NaCl, NaBr adopts either a rod-like or square morphology.

2.4 NaCl and NaI System

When internally mixed particles containing NaCl and NaI are imaged, we observe phase separation, in which the NaI forms a shell around a cubic NaCl core (Figure 5). Similar morphologies are observed at all ratios of NaCl to NaI.

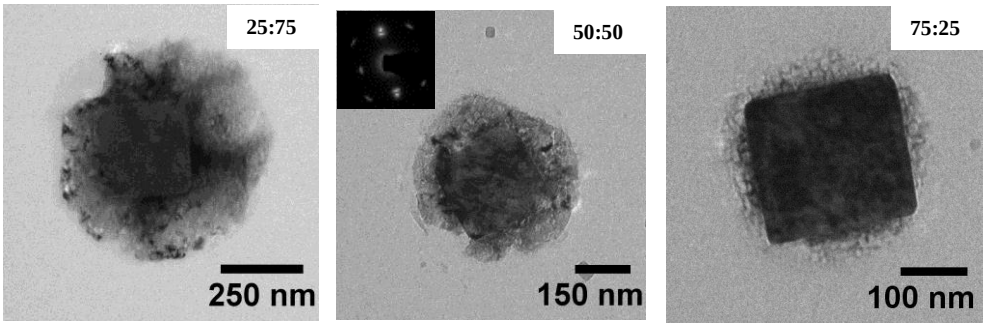

Figure 5: TEM images of binary mixtures of NaCl and NaI. The inset to the 50:50 image is the SAED pattern.

Unlike the NaCl/NaBr particles, the NaI shell of the particle does not appear to be a single-crystal. Phase separation was verified using EDS to obtain elemental composition at various locations on the particles. The spectra show enhancement of I on the outside of the particle and enhancement of Cl at the center of the particle, which is indicative of phase separation. While the majority of NaCl seems to be at the core of the particle based on EDS and the morphology, it is unclear if any NaCl is located at the shell of the particle as well. SAED images show both a single-crystal and polycrystalline

component as seen in the inset to the 50:50 mixture in Figure 5. The SAED image demonstrates that the NaCl had no effect on the crystallization of NaI with both single and polycrystalline diffraction patterns present. The calculated lattice spacings for NaCl and NaI were 5.64 and 6.46 Å, respectively. These values correlate well with the accepted lattice spacings of NaCl and NaI which are 5.627 and 6.462 Å, respectively.[30] These results suggest that the crystallization of NaCl (46% ERH) does not guide the crystallization for NaI (10% ERH). A reason for this is a mismatch in lattice spacings. NaI has a lattice spacing of 6.462 Å, much further from the lattice spacing of NaCl (5.627 Å) with a difference of 0.835 Å. The NaCl/NaBr system however has only a lattice difference of 0.323 Å; therefore, NaCl is able to guide the crystallization of NaBr. Although heterogeneous nucleation will be energetically favored over homogenous nucleation in the NaCl/NaI system, there remains a poor match in lattice spacings. Therefore, NaCl is not able to act as a template for the formation of NaI due to these discrepancies in lattice spacings.

2.5 Effect of surfactant on crystallization

We have also investigated the effect of surfactant on crystal growth using sodium dodecyl sulfate (SDS). Since fatty acids are ubiquitous at the ocean surface, they are incorporated into the aerosol particle during bubble-bursting. While SDS is not atmospherically relevant, it serves as a proxy for fatty acids found in the ocean and has been well-characterized and used in many studies.[31,32,33] We are interested how the incorporation of surfactants will affect the crystallization during efflorescence. Many studies have shown the incorporation of surfactant to have a variety of effects including the inhibition of water and gas-phase reactants from the gas phase into the particles.[34,35]

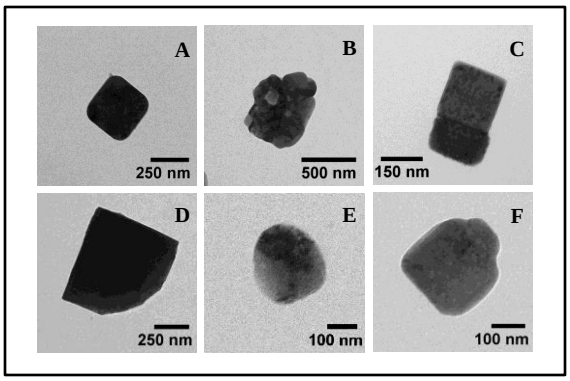

Figure 6. TEM images of (A) NaCl, (B) NaBr, (C) NaCl:NaBr 50:50, (D) NaCl + 1% SDS, (E) NaBr + 1% SDS, and (F) NaCl:NaBr 50:50 + 1% SDS.

We have investigated the effect of surfactant on NaCl, NaBr, and mixed particles. SDS was used as a proxy for soluble surfactants found in the ocean and was used at concentrations of 1 wt.%. The original structure of NaCl (Fig. 6a) is a cubic crystal with well-defined corners and edges. However, upon exposure to surfactant, the particles have a significantly different morphology with a general rounding of the particle edges. On some NaCl particles, the morphology is nearly spherical while on others, a well-defined corner is missing (Fig. 6d). Since NaBr is polycrystalline (Fig 6b), the effect of surfactant is less noticeable. However, particles with a more pronounced effect from the surfactant had a near-spherical morphology (Fig. 6e).

The effect of surfactant on the crystallization of internally mixed particles of NaCl and NaBr was also investigated for 50:50 mixtures of NaCl:NaBr. Compared to the unperturbed system, the addition of surfactant yielded a variety of morphologies. As shown in Fig. 6c, the NaCl and NaBr portions of the particle are well-defined with sharp contrast and corners. However, the effect of surfactant seems to disrupt the crystallization with the NaBr portion of the particle being significantly reduced or seemingly absent (Fig. 6f). The overall particle also adopts a more rounded morphology

with no well-defined edges on any of the particles imaged. Aggregation of particles was also observed to increase due to the presence of surfactant.

The results suggest that surfactants can significantly affect crystallization. The amount of surfactant used in this study (1 wt.%) was much less than the amount of organic occurring over oceans which ranges from 10-60 wt% demonstrating that only a small amount of organic compound is needed to observe these effects. Several studies have also shown with NO and NO_2 on a BaO surface and CO on MgO (001) that there is a general preference for adsorption at corner-sites. [36,37] Therefore, we can hypothesize that the organic molecules have a preferred adsorption at corner-sites.

2.6 Atmospheric Implications

Because particle morphology can impact heterogeneous chemistry, optical properties, water uptake, and ice nucleation; our results may have significant implications for atmospheric chemistry. The NaCl/NaBr system illustrates how in a multi-component particle the efflorescence of one component can influence the other components in a particle. Due to the match in lattice spacings, the particle has a morphology in which both the Cl and Br are accessible at the interface of the particle. Because both Cl and Br are accessible, both can readily participate in heterogeneous chemistry in the troposphere. In contrast, the NaCl and NaI system adopts a different structure due to the mismatch in lattice spacings. With a core-shell morphology, the coating of I must be chemically processed or diffused through before the Cl is exposed to atmospheric reactants and/or water. While the concentrations of NaBr and NaI used in this study are not atmospherically relevant, these results suggest the importance of lattice match in determining the resultant morphology of internally mixed particles composed of different

soluble inorganic components. Salts that effloresce in the atmosphere and have a cubic structure can be influenced by other salts if the lattice values are close in value. Salts that do not have a cubic structure such as ammonium sulfate, will also be much more complicated as the compound has multiple lattice constants. When comparing two different salts with multiple lattice constants (a,b, and c), if *ab* match and *ac* do not, then the salts may have a preferred orientation for growth. Therefore, even if one lattice constant does match with a salt, the other two lattice constants may not which could inhibit one salt from influencing another.

The experiments with SDS suggest that surface active organics significantly alter crystal growth. While SDS is not atmospherically relevant, it serves as a proxy for soluble surfactants which are ubiquitous at the ocean-air interface. The surfactant has critical effects on the morphology of the individual and mixed salt systems with particles having a more rounded morphology. It has been shown in numerous studies that surfactants can affect heterogeneous chemistry.[32, 38, 39, 40] A minor effect of these results is that it may also have implications for optical properties as the shape of the particle will have consequences for the interaction with incoming radiation.[41] Since satellites use optical properties to determine information such as the concentration of particles in the atmosphere, uncertainty in the morphology of the particle will inhibit accurate measurement of aerosol particle concentration. Through knowledge of particle morphology, better parameterizations for satellite retrievals and models can be developed allowing for more accurate determination of the atmospheric burden of aerosol particles.

Future experiments involve working with magnesium chloride. $MgCl_2$ is also found in the oceans but unlike the salts previously studied, it does not effloresce. Binary

mixtures of NaCl and $MgCl_2$ will be investigated at varying ratios to determine the morphology at varying concentrations. SAED will also be used on mixed salt and SDS systems to confirm disruption of crystal growth.

Chapter 3

Temperature Programmed Desorption

3.1 Surface Properties of Aerosol Particles and Ice Nucleation

Cirrus (ice) clouds cover approximately 20-35% of the globe and almost 50% of the tropics therefore having potentially a large influence on the radiation budget.[42, 43, 44] Cirrus clouds play an important role in the atmosphere by influencing water transport between the troposphere and lower stratosphere. They are also optically thin, allowing incoming radiation to enter and absorbing infrared radiation rising from the surface of earth causing a net warming effect.

Ice nucleation can either occur through homogenous freezing of liquid solution droplets or through heterogeneous freezing involving a particle nucleus. Homogenous freezing occurs typically at temperatures at or below -35 to -40 ^{0}C while the onset of heterogeneous freezing can occur at much warmer temperatures.[45] A particle can act as an ice nucleus by lowering the energy barrier to form ice. Zuberi et. al. found that the freezing temperatures of dust in ammonium sulfate solutions was 10 °C higher than ammonium sulfate solutions with no dust. [46] There are many hypothetical pathways, or modes, by which a particle can nucleate ice. One of these modes is known as deposition mode nucleation, which involves the formation of ice directly onto a solid surface from a supersaturated vapor environment.

While there have been many laboratory studies on ice nucleation,[47,48,49] there have been few studies on how the surface of a particle will affect its ice nucleating ability. Heterogeneous ice nucleation is thought to occur at specific "active" sites on a nucleating particle[50], and water exposure, surface chemical reactions, and organic coatings can all

affect how particles nucleate ice due to the surface structure of a particle changing. The adsorption of these substances to a surface can also have consequences for heterogeneous chemistry in the atmosphere. Depending on the strength of the adsorbate-substrate interactions, the adsorption of compounds to the surface of particles can affect the concentrations of that substance and hence the chemistry that occurs in the atmosphere.

A common constituent detected in the upper troposphere is ammonium sulfate.[51, 52] Ammonium sulfate is a hygroscopic salt that has also been shown to be an efficient ice nucleus in cirrus cloud particles.[53] By understanding how the surface of a particle affects ice nucleation, the formation and effects of cirrus clouds on our climate can be better evaluated. Increasing our knowledge on the adsorption and desorption of water and organic compounds from surfaces is also necessary to better understand gas-surface interactions and hence the chemistry of the troposphere. Since the chemical reactivity of ionic crystal surfaces can be altered by the presence of water, determining the energetics of water on surfaces is important for understanding these chemical processes.[54]

We have studied sodium chloride single crystals which serve as a proxy for tropospheric aerosols with soluble inorganic components. We have chosen sodium chloride since it is a hygroscopic salt that has been well-studied in surface science systems and is commercially available.

3.2 Experimental and Sample Preparation

The investigation of NaCl surfaces can be achieved using an Ultrahigh Vacuum (UHV) chamber which offers a precisely controlled environment with *in situ* atomic force microscopy (AFM), Fourier transform infrared spectroscopy (FTIR), and quadrupole mass spectrometry (MS). The UHV instrument is comprised of three different sections

separated by gate valves: the load-lock, the microscope chamber, and the preparation chamber (Figure 7).

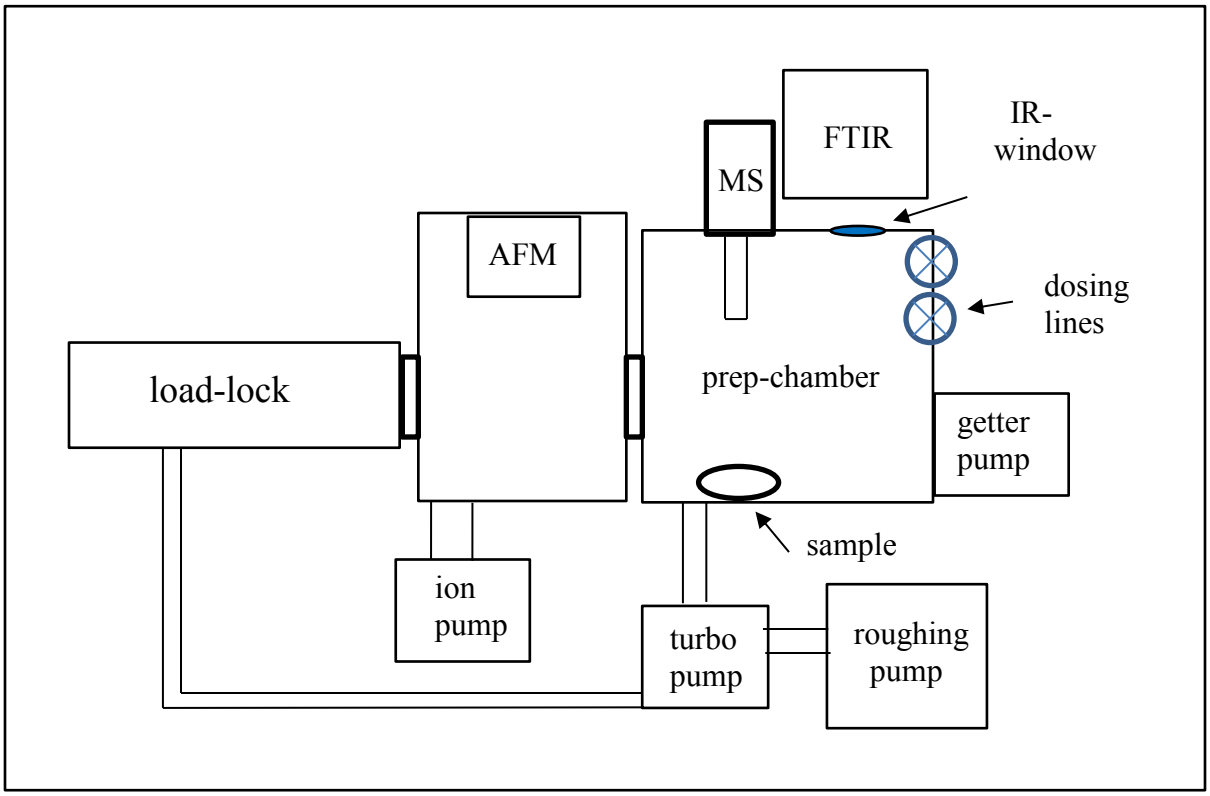

Figure 7. Schematic of the Ultra High Vacuum instrument.

Temperature programmed desorption (TPD) studies take place in the preparation chamber which houses a quadrupole mass spectrometer (QMS; Residual Gas Analyzer SRS 300). The preparation chamber is maintained by a roughing and turbo pump with a base pressure of approximately 1 X 10^{-9} Torr, as monitored by an ionization gauge.

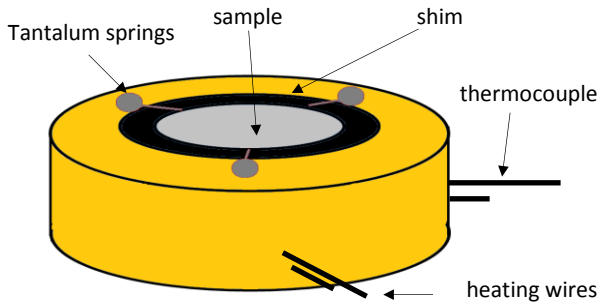

Figure 8. Schematic of the sample mount.

In a typical experiment, samples are first be prepared by cleaving NaCl (100) *ex situ* using a razor blade. The thin sample is placed between a series of shims and held in position by three Tantalum leaf springs (Figure 8). The sample holder also contains a filament made of 0.006'' tungsten wire. This filament allows us to apply up to 3.5A of current to the sample to be radiatively heated to the desired temperature. The sample also sits on a K-type thermocouple for the measurement of temperature. The heating of the sample is controlled by a Heat2-Power Supply system (Precision and Vacuum Technology). We have developed a LabView program that integrates the temperature with the pressures obtained from the mass spectrometer.

To cool the sample, N_2 gas (< 2 ppm moisture) was passed through a ¼ in. copper coil immersed in liquid nitrogen. This coil is connected to the inlet of the preparation chamber and allowed for rapid cooling of the sample.

The prepared sample is introduced into the chamber through the load lock and passed through the instrument using a transform arm to the preparation chamber. Connected to the preparation chamber are several leak valves for sample dosing via chamber back-filling. Desorbing molecules from the sample are detected using the mass spectrometer. The ionization volume of the mass spectrometer is enclosed in a home-built stainless steel Feulner cap (Figure 9).[55]

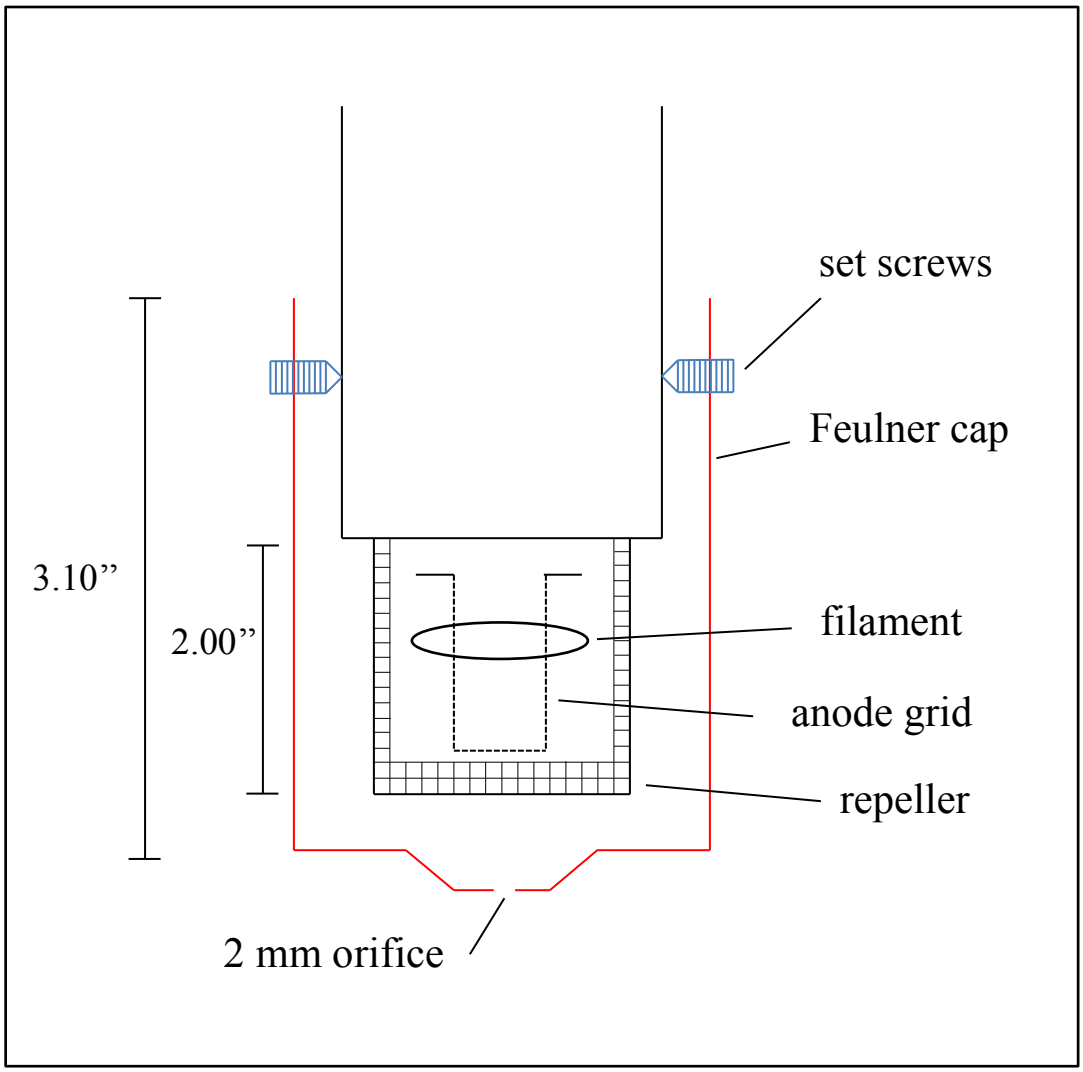

Figure 9. The schematic of the Feulner cap which houses the filament of the mass spectrometer. The 2 mm orifice of the cap is placed close to the sample for the detection of desorbing molecules.

The Feulner cap contains a small orifice (2 mm) placed close to the sample surface to allow for desorbing molecules to reach the ionizer. This setup offers several advantages. It effectively excludes substances desorbing from other components in the chamber from reaching the ionizer therefore limiting detection to only the sample.

In a typical experiment, several background measurements are performed. The sample is typically cooled to temperatures ranging from 90 to 100 K and heated to roughly 300 K since no high temperature peaks are observed. The Feulner cap is

retracted to allow water to easily adsorb to the sample. Exposure is measured in units of Langmuir, where 1 Langmuir (1 L) = 10^{-6} Torr s. After dosing, the Feulner cap is then brought close to the sample and the TPD spectra were recorded at a heating rate of 35 K/min (0.583 K/s). Systems that are investigated include: NaCl and water, calcite and water, and graphite and water.

3.3 TPDS Data and Analysis Techniques

Temperature programmed desorption (TPD) is a useful tool to investigate the bonding of adsorbates to surfaces. Temperature programmed desorption measures the temperature dependence of the desorption process of an adsorbate on a surface. Monitoring both temperature and pressure, a TPD spectra can be obtained from which much information can be obtained. The technique can provide the activation energy for desorption, the desorption mechanism, and information regarding adsorbate-adsorbate interactions.

A typical desorption spectrum contains peaks or features that correspond to the type of binding site to the surface. The area under the desorption spectrum is also the coverage of the adsorbate on the surface. The temperature at peak-maximum and the kinetic mechanisms of the desorption can be used to determine the activation barrier for desorption, E_{des}, or the enthalpy of desorption (binding energy). If the activation energy barrier for adsorption is assumed to be zero, the activation energy and binding energy can be directly found from the TPD data.[56]

Desorption processes can occur through either zero, first, or second order kinetics. The desorption mechanism in many cases can be determined by observing how the temperature at peak maximum changes as coverage is increased. However, if there are

strong attractive or repulsive interactions between the adsorbate molecules, then E_{des} is dependent on coverage. If the activation energy decreases with coverage for a process that is first-order, the temperature at peak maximum will decrease in temperature which could be mistaken for a second order process.[55] Therefore, the shape of the peak should also be taken into consideration as well (Figure 10).

Zeroth order kinetics is typical of evaporation from multilayers of adsorbate on a surface such as the desorption of Cu multilayers from Ru (0001).[57] The temperature of peak maximum increases as coverage increases and the peaks share a common leading edge. Pseudo-zeroth order could also occur if there are strong attractive interactions between the adsorbates.

First-order kinetics is most commonly observed and is characteristic for molecular desorption such as CO desorption from Pd(100).[58] The temperature of maximum desorption occurs at the same temperature for each coverage. The shapes of the curves are typically asymmetric with a steady slope up and a rapid fall after the peak maximum.

Second-order processes are observed when recombination processes occur between atomic species such as hydrogen desorbing from Ni (100).[59] The temperature of maximum desorption decreases as coverage increases and peak shapes are typically symmetrical. Pseudo-second order desorption can also occur if there are strong repulsive adsorbate-adsorbate interactions.

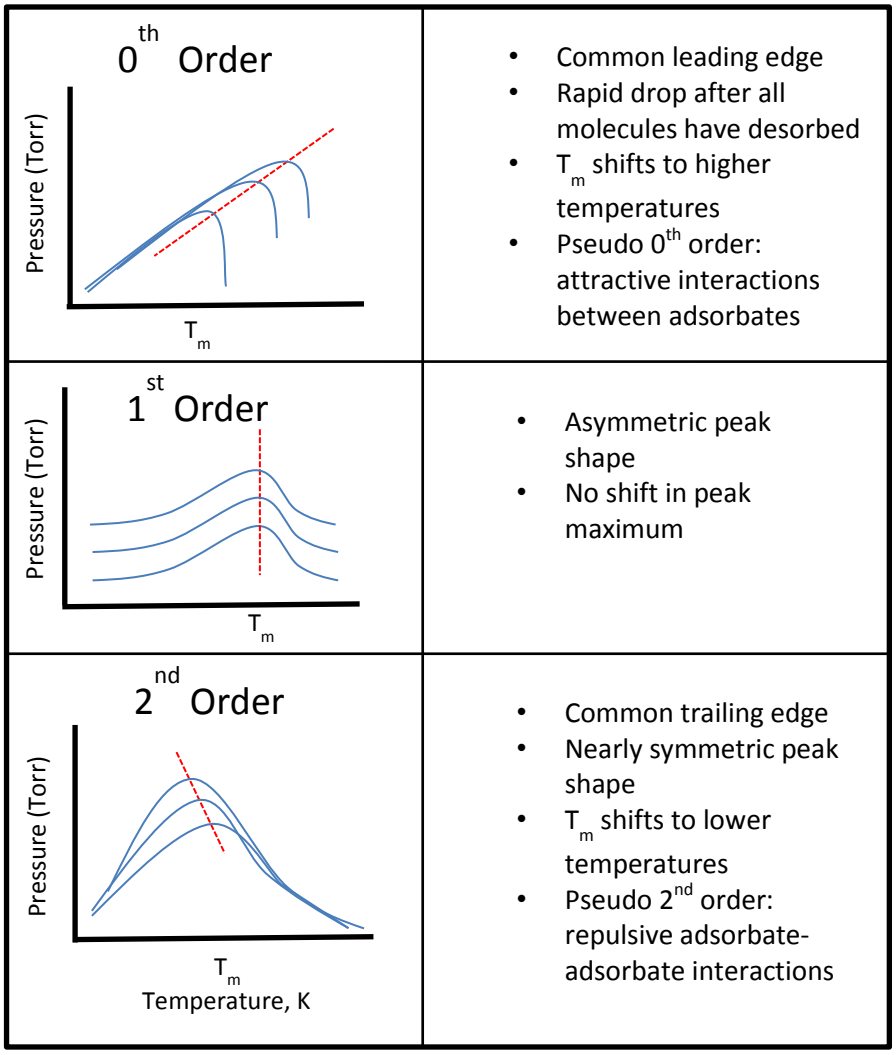

Figure 10: A summary of the kinetic mechanism information obtained from TPDS spectra.

The broadness of a peak can also provide information on the hydrophilicity of the substrate. Grimm et al.[60] studied the desorption of water from alkane thiol self-assembled monolayers (SAM) with both hydrophilic, hydrophobic, and mixed terminal groups using TPDS. The study found that desorption from a pure carboxylic acid-terminated surface produced broad peaks and desorption at higher temperatures due to stronger interactions with the surface. In contrast, a methyl-terminated SAM produced narrower peaks with desorption at much lower temperatures.

To determine quantitative information such as the desorption rate, r, and the activation energy for desorption, E_{des}, the spectra can be analyzed using the Polyani-Wigner equation[61],

$$r = -\frac{d\Theta}{dt} = v(\Theta)\Theta^n \, exp(-\frac{E_{des}(\Theta)}{RT}) \qquad \text{Equation 2}$$

where, Θ is the coverage in monolayers, t is time, n is the order of desorption, ν is the pre-exponential/frequency factor, R is the gas constant, and T is the temperature.

There have been a variety of simplified analysis methods for TPDS developed including Redhead analysis.[62] This analysis assumes that desorption follows first order kinetics and that E_{des} and ν are independent of surface coverage. With these assumptions, such analysis yields,

$$\Delta E_{des} = RT_{max}[\ln \frac{\nu_1 T_{max}}{\beta} - \ln \frac{\Delta E_{des}}{RT_{max}}] \qquad \text{Equation 3}$$

where T_{max} is the temperature at maximum desorption, β is the heating rate, and ν_1 is the frequency factor. The value for the second part of the brackets in Equation 3 is smaller than the first term and is estimated to be 3.64 yielding[61],

$$\Delta E_{des} = RT_{max}[\ln \frac{\nu_1 T_{max}}{\beta} - 3.64] \qquad \text{Equation 4}$$

An approximate value for ν_1 of 10^{13} s^{-1} is also chosen. There are several cases where the assumption of first-order kinetics is not valid such as with porous particles as well as if readsorption occurs. However, readsorption can be negligible under high vacuum conditions.[63] Redhead analysis is a good first approximation and has been used widely in many studies regardless of the desorption order.

3.4 The Feulner cap

Before the implementation of the Feulner cap, the TPDS spectra had too many peaks and irregularities. Since the entire chamber is backfilled with water vapor, other

components in the chamber are exposed to water vapor. Therefore, when performing TPDS, the mass spectrometer was detecting water desorbing from the sample mount and other components in the chamber.

To increase the sensitivity to the desorption from the sample, an aluminum Feulner cap was designed. Aluminum was chosen initially since it is easy to machine. The aluminum Feulner cap was effective at limiting the amount of peaks and irregularities in the spectra. However, there were no distinguishing features in the spectra to indicate the desorption of water. Gases were also accumulating in the Feulner cap which suggested that there was not enough conductance within the cap for the gases to be pumped away.

To alleviate the issues experienced with the aluminum Feulner cap, the next cap was designed using stainless steel which is more commonly found in vacuum systems. The design was also modified to make the walls thinner to allow for higher conductance.

3.5 TPDS of water on NaCl

The first system of study was the adsorption of water on NaCl. The mass to charge ratio (m/z) monitored in these experiments is 18 (H_2O^+). As shown in Figure 11, desorption of low exposures (1 L) of water from NaCl is characterized by a sharp peak centered at 156.15 ± 0.32 K and a broad peak at 180.99 ± 3.03 K. The presence of peak A at low coverages suggests that the formation of the first monolayer is accompanied by the formation of water clusters at step edges on the surface.

The low temperature peak (labeled A) does not shift with increasing dosage to 2 L which is indicative of first-order desorption. The high temperature peak (labeled B) shifts to higher temperatures as coverage increases which is suggestive of zeroth-order

desorption. Since the weakest bonds desorb at lower temperatures, we expect peak A to be a result of desorption of water primarily from water on the surface. Since peak B is broader and desorbs at higher temperatures, we propose this peak is attributed to the desorption of water from NaCl. We expect the electrostatic interactions between Na and water to be stronger than water-water interactions.

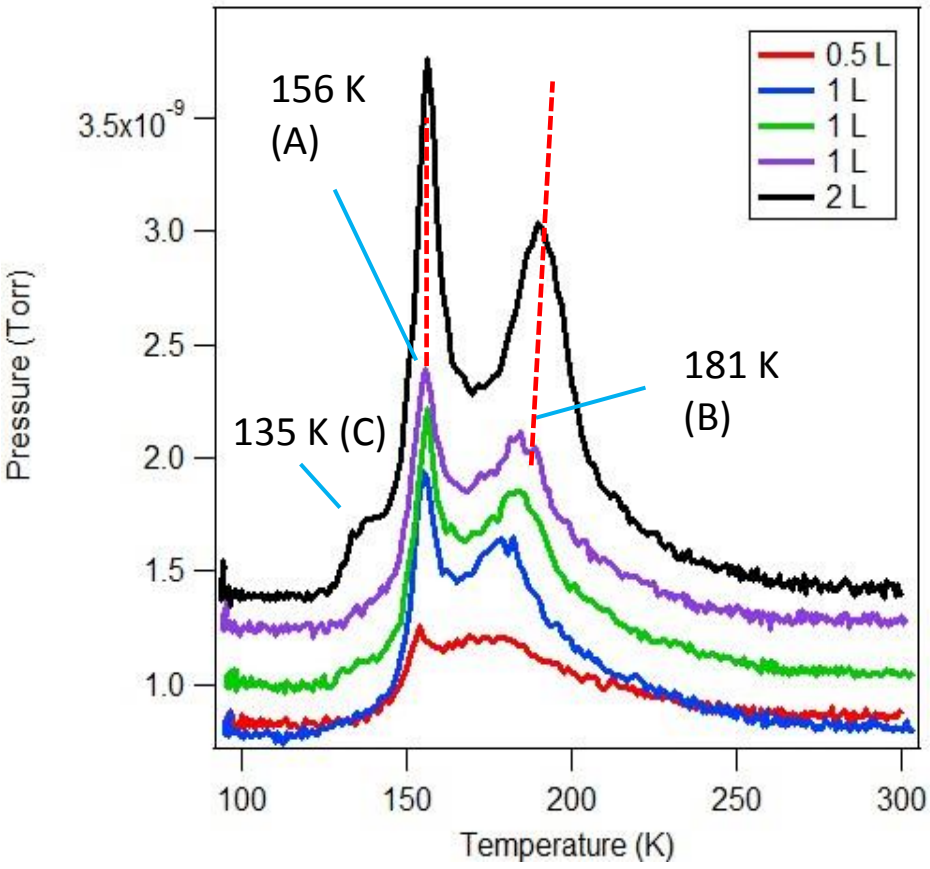

Figure 11: The thermal desorption spectra of low doses of water adsorbed on NaCl (100). The sample was cooled to 90 K, dosed with water, and heated at a rate of 35 K/min.

At exposures greater than 1 L, a second low-temperature peak occurs at about 135 K (labeled C). This feature becomes more distinct with increasing coverage and slightly shifts in temperature as temperature increases (Figure 12). At higher exposures (16 L) feature C becomes a shoulder of peak A.

Other studies have observed a similar peak and have attributed it to the transition from amorphous solid water to crystalline ice. Since we are dosing at low temperatures (~100 K), we are forming amorphous solid water (ASW) at the surface which undergoes a transition to crystalline ice at approximately 135 K. [64,65] During this transition, the vapor pressure changes and hence the desorption rate which causes a bump in the spectrum. This transition has typically been observed between the temperatures of 130 and 160 K.[66,67] Enguist et al.[68] examined the desorption of D_2O from mixed alkanethiolate self-assembled monolayers (SAMs) on gold with both hydrophilic and hydrophobic properties. They found that the transition of D_2O from amorphous to crystalline depended on the functional groups present on the surface with a transition temperature near 110 K for the hydrophobic (CH_3) surface and 150 K for hydrophilic (OH) surface. A previous study that analyzed both H_2O and D_2O on Pt(111) found only a 4 K difference in the peak maximum in the desorption spectrum.[69]

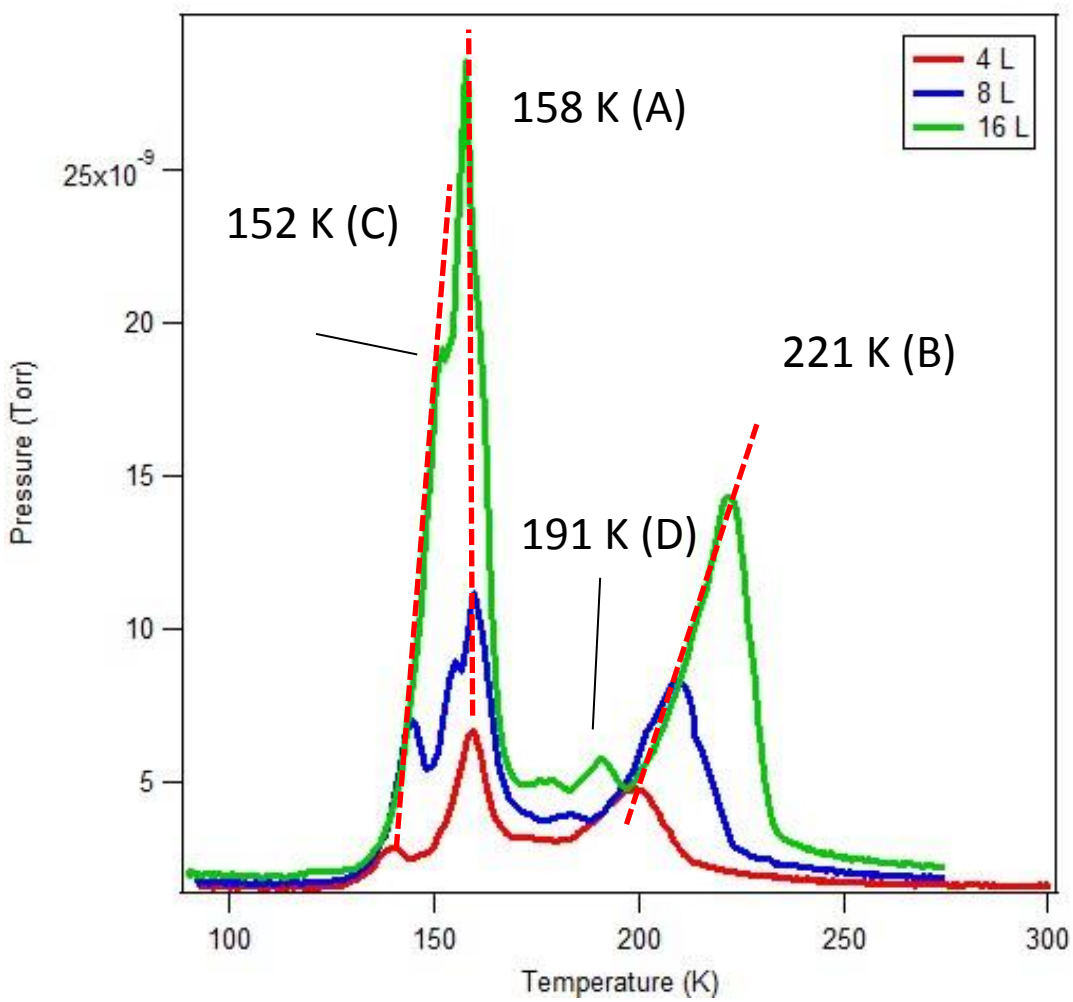

Figure 12: The thermal desorption spectra of high doses of water adsorbed on NaCl (100). The sample was cooled to 90 K, dosed with water, and heated at a rate of 35 K/min.

Quantitative analysis was performed for the low-coverage desorption traces including peaks A and B. Redhead analysis was performed on the 1 L peaks yielding 42.96 ± 2.64 kJ/mol and 50.06 ± 4.05 kJ/mol for peaks A and B respectively.

If peak A is the desorption of multilayers, then it is slightly less than the literature value for the sublimation of water ice which is of 50.95 kJ/mol.[70] This discrepancy in values is expected as the surface will influence the sublimation of ice. If peak B is a result from the desorption of water from the surface of NaCl then our value does fall in

between the reported binding energies of water to NaCl which range from 41.84 to 62.76 kJ/mol.[71 ,72]

Previous studies have shown that at submonolayer coverages, water primarily interacts with Na^+ at the surface. After about 0.5 ML, water-water interactions are favored over water-surface bonds.[73, 74] This can be seen in the 0.5 L trace in Figure 11 with two peaks present. To confirm our peak assignments, we will perform experiments with coverages less than 0.5 L to more accurately determine the peak assignments.

To examine the evolution of the desorption features with increasing exposures, dosages of 4, 8, and 16 L were also investigated (Figure 12). The maximum of peak A in the desorption spectrum does not undergo significant shift in temperature with increasing coverages; still exhibiting first-order desorption. Peak A dominates at the highest coverages which is typical of multilayer desorption. Alternatively, peak B continues to shift to higher temperatures with increasing coverage. Peak B is also comparatively broad compared to the other peaks suggesting a large number of adsorption sites.[75] Peak B could be exhibiting properties of zeroth-order desorption or the activation energy for desorption increases with coverage causing a shift in the temperature of maximum desorption. At 8 L, a small feature appears between peaks A and B and becomes more prominent at dosages of 16 L centered at approximately 191 K (labeled D). This feature shifts to higher temperatures and becomes more pronounced with even higher dosages of 32 L (not shown). This feature is possibly due to desorption from water in a second layer. Several studies have detected the presence of a strongly bound second layer in their desorption spectra.[75, 76] Another possible assignment to peak D is the transition from cubic crystalline ice to hexagonal ice which occurs around 200 K.[77, 78]

The low exposures of water were performed again on the same salt sample, which had already undergone high exposures of water during the previous study. For low doses (1 L), peak A was shifted to lower temperatures at 148.31 ± 0.13 K and peak B was shifted to higher temperatures at 197.10 ± 1.84 K compared to Figure 11. It is possible that the water adsorbing to the sample during the first day of study is etching the surface which subsequently would affect the desorption features in the spectra. In a previous study, Salmeron et al.[79] has found that the adsorption of water caused significant changes at the NaCl surface using atomic force microscopy. When NaCl was exposed to relative humidities greater than 35%, the step edges were observed to move on the surface. While these exposures were much higher than what we are dosing, this could offer an explanation as to why the desorption features in the spectrum shift in temperature from day to day after exposure to water. This behavior was also observed for another fresh salt sample that was studied on two different days. The first day of study had similar values to the features seen in Figure 11 and underwent similar shifts in temperature maximum when studied on a separate day.

To explore this possibility, we coupled our TPDS experiments with our AFM. A fresh salt sample was imaged and TPDS experiments were carried out in which low and high exposures of water were performed. Images were taken between TPDs experiments to examine the effects of water adsorbing and desorbing from the surface.

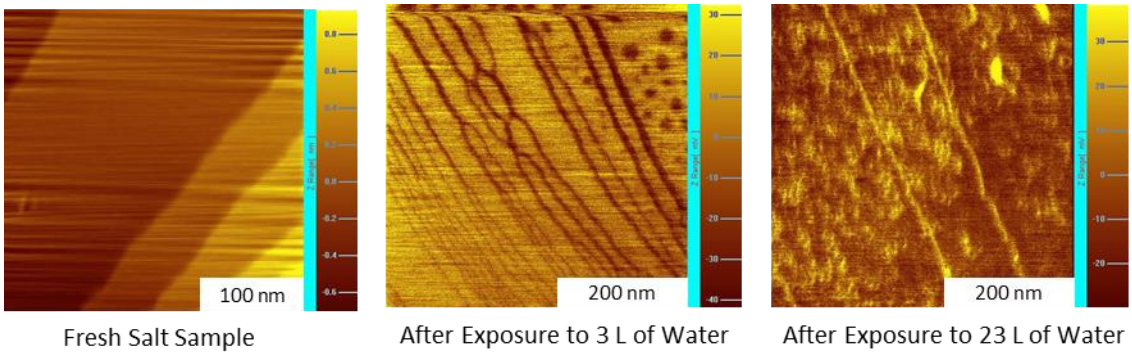

Figure 13: AFM images of freshly cleaved NaCl, after exposure to 3 L of water, and after exposure to 23L of water respectively.

The freshly cleaved NaCl sample has well-defined step edges as expected (Figure 13). After exposures and desorption of 3 Langmuirs of water, we notice pitting on the surface. After higher exposures of water (23 L), we notice a higher density of defects. The increase in defects with exposures to water can possibly offer an explanation as to why the peaks in the TPD spectrum shift to warmer temperatures sequentially over several days of performing studies on the same sample. Water appears to be causing more defects on the surface allowing stronger Na^+ -water interactions.

3.6 Water on Calcite

To investigate a less hygroscopic surface, the adsorption of water to calcite was studied under similar experimental conditions. Calcite is a common mineral found in the environment and serves a proxy for minerals in the atmosphere. While it is not the best proxy mineral since it is only a minor component by weight of airborne mineral dust[80], it is easy to work with in vacuum systems since it can be cleaved easily. Calcite was exposed to water at roughly 90 K and heated at a rate of 35 K/min (Figure 14).

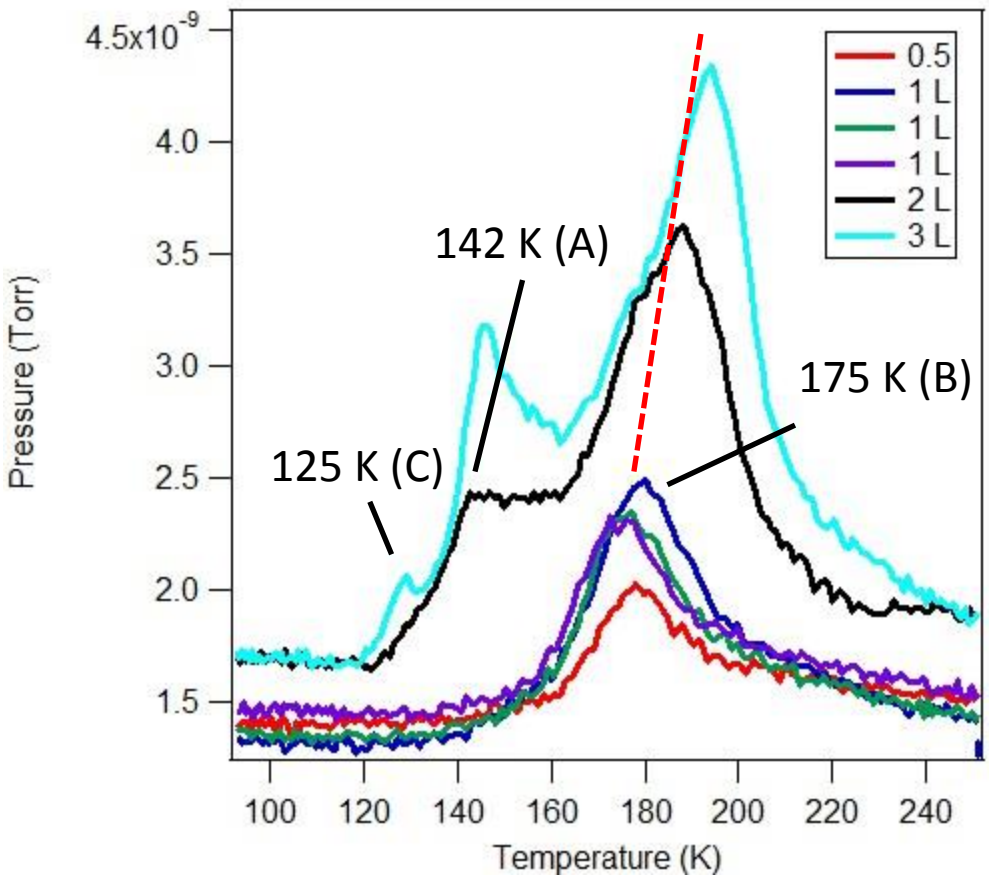

Figure 14. The thermal desorption spectra of low doses of water adsorbed onto calcite. The sample was cooled to 90 K, dosed with water, and heated at a rate of 35 K/min.

At the lowest coverages, the desorption profile consists of a single broad peak centered at approximately 175 K (labeled B). For coverages ≤ 1 L, the maximum temperature does not change with coverage suggesting first-order desorption. However, at 2 L, this peak shifts to 186.85 K and a new feature appears at 141.79 K (labeled A). This peak is most likely due to multilayer desorption. As coverage increases, the shoulder manifests itself into a well-defined peak that increases in temperature with coverage. At 3 L, a new feature appears (labeled at C) at approximately 125 K. Similar to the NaCl system, this is probably due to the transition of amorphous solid water to crystalline ice.

Redhead analysis of the 0.5 L and 1 L desorption profile for Peak B yields desorption energies of 47.08 kJ/mol and 46.73 kJ/mol respectively. Previous studies using atomistic simulation techniques found binding energies of about 92.2 kJ/mol for water on calcite.[81]

Previous studies have shown that with water on calcite; strong adsorbate-substrate interactions disrupt any hydrogen bonding of the first monolayer. Therefore, unlike the NaCl system, calcite forms a complete monolayer of water before water-water interactions begin. This is reflected in the TPDS spectra as there is only one peak for 1 L and two peaks for the 2 L trace. [82]

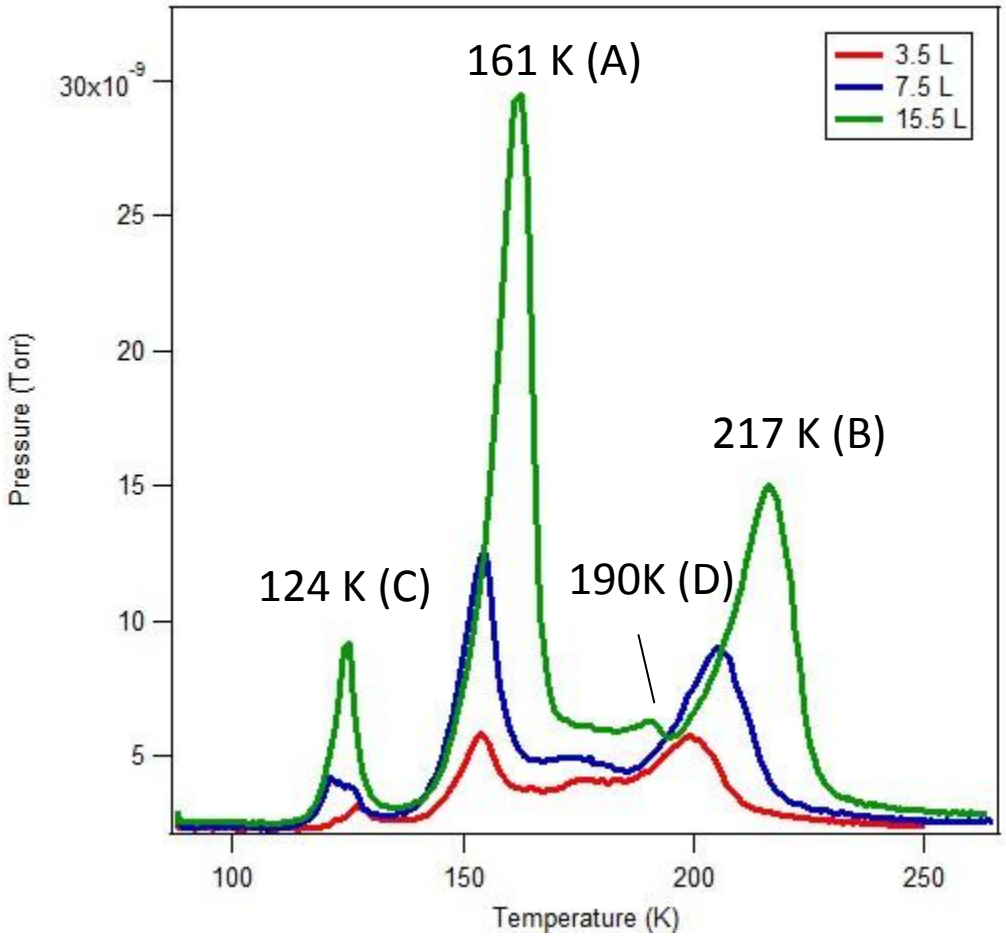

Figure 15. The thermal desorption spectra of high doses of water adsorbed onto calcite. The sample was cooled to 90 K, dosed with water, and heated at a rate of 35 K/min.

Further exposing the calcite to higher doses of water causes more features in the spectra (Figure 15). Peak C becomes more pronounced and the temperature of maximum desorption increases with increasing coverage. Peaks A and B also generally shift to higher temperatures with increasing coverage as well which is suggestive of zeroth order desorption. Increasing the exposure to 15.5 L shows a new peak that forms at approximately 190 K (labeled D). Peak D shifts to higher temperatures with increasing coverage which suggests zeroth order. Similar to the NaCl results, this could be a result from either desorption from the second layer of water or the transition from cubic crystalline to hexagonal ice.

3.7 TPDS of Water on Graphite

To investigate the water desorption from a hydrophobic surface, water was desorbed from highly ordered pyrolytic graphite (HOPG). The desorption spectra of water from graphite includes two distinguishable states at approximately 124 K and 210 K labeled A and B respectively (Figure 16).

Based on previous studies of water on HOPG, it was shown that water grows by a cluster growth mechanism with island formation.[83, 84, 85]

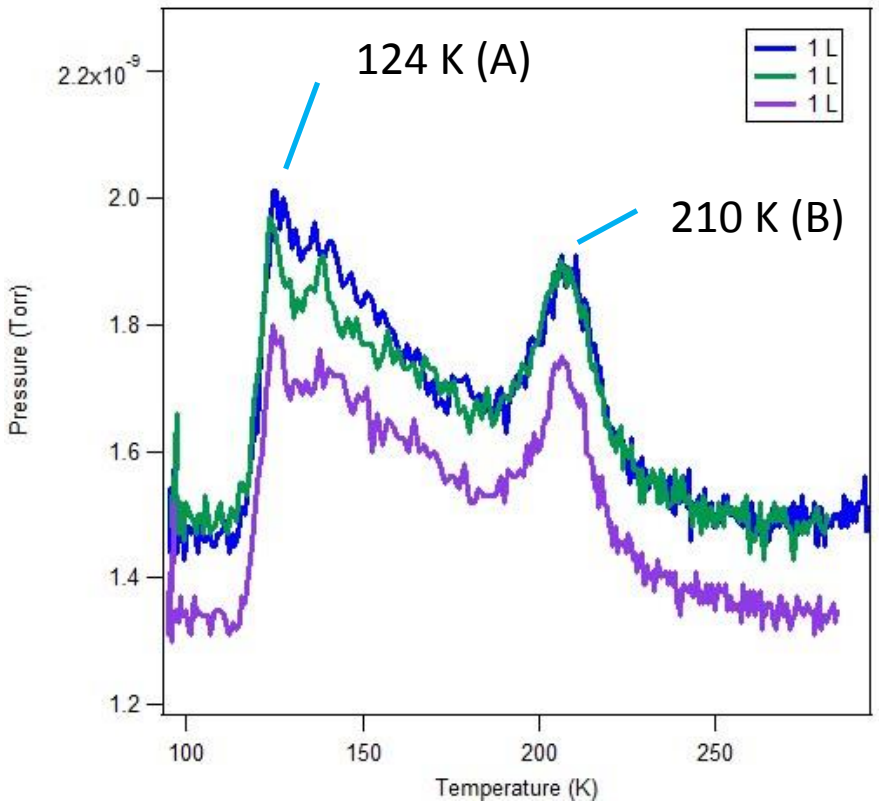

Figure 16. The thermal desorption spectra of low doses of water adsorbed onto graphite. The sample was cooled to 90 K, dosed with water, and heated at a rate of 35 K/min.

Based on these results, it is possible to assign the peaks in our spectra (Figure 16). The low-temperature peak is due to weak water –graphite interactions. The high temperature peak centered at 210 K is possibly due to water-water interactions.

Redhead analysis of these two peaks yields desorption energies of 32.57 kJ/mol and 56.10 kJ/mol respectively for 1 L. Clemens et al. [86] examined water desorption from graphite and found a binding energy range of 30.87 to 39.50 kJ/mol for water desorption from the edges or surface of islands on graphite depending on the sample preparation. This value matches our calculated desorption energy value for Peak A.

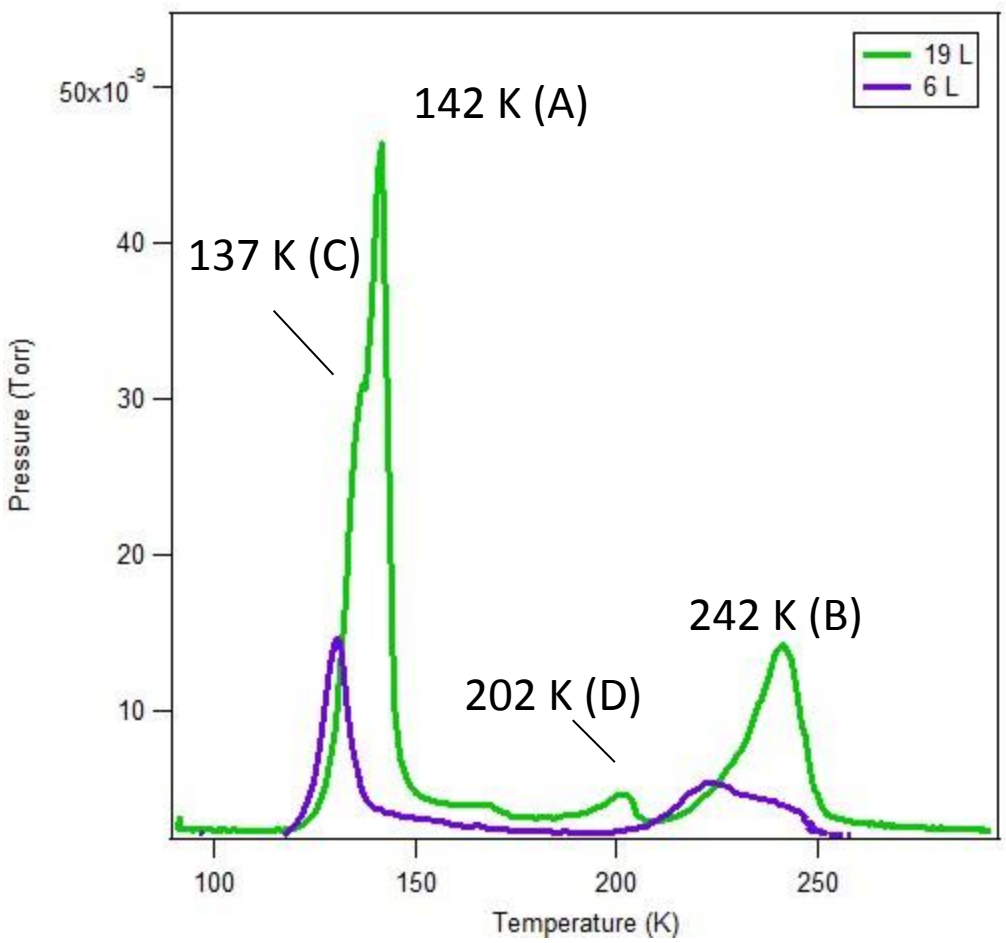

Figure 17. The thermal desorption spectra of high doses of water adsorbed onto graphite. The sample was cooled to 90 K, dosed with water, and heated at a rate of 35 K/min.

As the coverage is increased, both peaks A and B continue to shift to higher temperatures which indicates zeroth order desorption (Figure 17). At 19 L, peak A develops a slight shoulder at approximately 136 K which could be the transition from amorphous solid water to crystalline ice. A feature at 202 K also appears at 19 L and can be attributed to the transition of cubic crystalline ice to hexagonal ice. Alternatively, it could also be desorption from the second layer of water. Both Peak C and D shift to higher temperatures with coverage which is suggestive of zeroth order desorption.

3.8 Summary and Atmospheric Implications

System	Assignment (Θ) = 1 L)	T_{max} (K)	E_{des} (kJ/mol) (Redhead Analysis)
NaCl	Water interaction directly with surface	181	50.06
Calcite	Water interaction directly with surface	175	46.73
Graphite	Water desorption from water islands on graphite surface	124	32.57

Table 1: A comparison of the different desorption energies of water from the surfaces used in this study.

Determining the binding energy of water to these surfaces will provide insight into ice nucleation. If water has a high affinity for a surface, we expect ice nucleation to occur at lower supersaturations. While this data is still preliminary, it can provide some insight into how the surface may act as an ice nucleus. From the TPDS data we obtained (Table 1), it can be seen that water has the strongest interaction with NaCl. Since water is bound strongest to NaCl, we would expect NaCl to serve as the best ice nucleus. Many studies have also shown NaCl to be an efficient ice nucleus.[87,88] We also expect graphite to be the least efficient ice nucleus due to its weak interaction with water. One study had investigated n-hexane soot, a different hydrophobic surface, and found that the onset for ice nucleation with n-hexane soot did not differ from the substrate alone.[89] Therefore, graphite is expected to be a poor ice nucleus.

Thin films of water on surfaces can have consequences for heterogeneous chemistry in the atmosphere. Since NaCl has the strongest interaction with water, consequences for heterogeneous chemistry would be more pronounced than for calcite or graphite systems. Water bound to the surface can alter the chemical reactivity therefore having a stronger effect for NaCl rather than graphite.

3.9 Future Directions

Future investigations with temperature programmed desorption include performing further studies of water desorption from NaCl, calcite, and graphite surfaces. The current data obtained is preliminary and further trials are necessary. We will perform exposures less than 0.5 L and increase at 0.5 L increments to help determine how the desorption profiles change as the coverage increases. This will help determine peak assignments as well as whether a desorption process is zeroth, first, or second-order.

Performing other types of analysis besides Redhead analysis will also be helpful in determining activation energy, reaction order, and the frequency factor. Redhead analysis is a good first approximation but performing full quantitative analysis is necessary to determine more accurate values.

One useful method, known as the heating variation method, involves varying the heating rate (β) by more than two orders of magnitude for the same coverage.[90] The temperature at peak maximum (T_p) is determined for each heating rate and $\ln (\beta / T_p^2)$ vs. $(1/T_p)$ is plotted. This should produce a straight line with slope of $-E_{des}/R$ with the only assumption that E_{des} is independent of coverage. If coverage is known, an accurate frequency factor can be determined. If there are strong adsorbate-adsorbate interactions, deviations from linearity will be observed in this method.

A complete analysis of TPD spectra, first proposed by King[91], involves determining E_{des} and ν for each coverage since these two values can depend on coverage. An arbitrary coverage is chosen (θ') and points that correspond to this coverage are

determined for all the TPD curves with coverages greater than Θ'. This provides a set of values which are plotted as ln p versus 1/T. E_{des} can be determined from the slope and the prefactor from the y-intercept.

Another type of analysis is leading edge analysis.[92] This analysis is based off the logarithmic Polanyi-Wigner equation,

$$\frac{d\ln(\frac{d\Theta}{dT})}{d(\frac{1}{T})} = \frac{d\ln(p)}{d(\frac{1}{T})} = -\frac{\Delta E_{des}}{RT} + \ln v + n\ln(\Theta) \qquad \text{Equation 5}$$

where p is the pressure, v is the frequency factor, and Θ is the coverage. With this analysis, a small section of the spectrum on its leading edge is selected to keep temperature and coverage constant. Therefore, a plot of ln p versus 1/T will give a straight line with slope of $-E_{des}/R$. An advantage of this method is that there are few assumptions. However, the leading edge of a peak may be in a region of low signal to noise making this analysis difficult.

To explore the effect of water possibly etching the surface, we will continue to use AFM to determine if water is etching the surface after low exposures (1L) are desorbed from the sample surface. If significant defects are observed on the surface, this can explain the shift in temperatures observed in the TPD spectra from day to day.

Chapter 4

Conclusions

4.1 Conclusion

Transmission electron microscopy and energy dispersive X-ray spectroscopy are used to investigate the morphology of single and binary component particles comprised of salt compounds. Understanding the shape of sea salt aerosols in the troposphere is important as the morphology of particles can have many consequences for heterogeneous chemistry, optical properties, water uptake, and ice nucleation. A UHV instrument with mass spectrometry and AFM capabilities was also used to investigate surface properties of aerosol particles and the adsorbate-substrate interactions using TPDS and AFM. Evaluating how water adsorbs to the surface will help characterize what substances will affect water adsorption and ice nucleation in the upper layers of the troposphere. Increased knowledge of the morphology and surfaces of aerosol particles will lead to a better understanding of heterogeneous atmospheric processes.

References

[1] Albrecht, B. Aerosols, cloud microphysics and fractional cloudiness. *Science* **1989**, *245*, 1227-1230.
[2] Twomey, S.A. The influence of pollution on the shortwave albedo of clouds. *J. Atmos. Sci.* **1977**, *34*, 1149-1152.
[3] Bernstein, J.A.; Alexis, N.; Barnes, C.; Bernstein, I.L.; Nel, A.; Peden, D.; Diaz-Sanchez, D.; Tarlo, S.M.; Williams, P.B. Health Effects of Air Pollution. *J. Allergy Clin. Immunol.* **2004,** *114*, 1116.
[4] Samet, J.; Wassel, R.; Holmes, K.J.; Abt, E.; Bakshi, K. Research Priorities for Airborne Particulate Matter in the United States. *Environ. Sci. Technol.* **2005,** *39*, 209A.
[5] Forster, P.; Ramaswamy, V.; Artaxo, P.; Bernsten, T.; Betts, R.; Fahey, D.W.; Haywood, J.; Lean, J.; Lowe, D.C.; Myhre, G.; Nganga, J.; Prinn, R.; Raga, G.; Schulz, M.; Van Dorland, R. 2007: Changes in Atmospheric Constituents and in Radiative Forcing. *In: Climate Change 2007: The Physical Sciences Basis. Contribution of Working Group I to the Fourth Assessment Report of the Intergovernmental Panel on Climate Change* [Solomon, S., D. Qin, M. Manning, Z.Chen, M.Marquis, K.B. Averyt, M.Tigmor and H.L. Miller (eds.)]. Cambridge University Press, Cambridge, United Kingdom and New York, NY, USA.
[6] Blanchard, D.C.; Woodcock, A.H. The production, concentration and vertical distribution of the sea salt aerosol. *Ann. N.Y. Acad. Sci.* **1980**, *338*, 330-347.
[7] Sievering, H.; Boatman, J.; Gorman, E.; Kim, Y.; Anderson, L.; Ennis, G.; Luria, M.; Pandis, S. Removal of sulfur from the marine boundary layer by ozone oxidation in sea-salt aerosols. *Nature* **1992,** *360*, 571-573.
[8] Holmes, C.D.; Jacob, D.J.; Yang, X. Global lifetime of elemental mercury against oxidation by atomic bromine in the free troposphere. *Geophys. Res. Lett.* **2006**, *33*, L20808.
[9] Read, K.A.; Mahajan, A.S.; Carpenter, L.J.; Evans, M.J.; Faria, B.V.E.; Heard, D.E.; Hopkins, J.R.; Lee, J.D.; Moller, S.J.; Lewis, A.C.; Mendes, L.; McQuaid, J.B.; Oetjen, H.; Saiz-Lopez, A.; Pilling, M.J.; Plane, J.M.C. Extensive halogen-mediated ozone destruction over the tropical Atlantic ocean. *Nature*. **2008**, *453*, 1232-1235.
[10] Lewis, E.R.; Schwartz, S.E. *Sea salt aerosol production: mechanism, methods, measurements and models*, geophysical monograph series; American Geophysical Union : Washington, D.C., 2004; 37.
[11] Rapp, R.J.; Melville, W.K. Laboratory measurements of deep-water breaking waves. *Philos. T. R. Soc. Lond.* **1990**, *331*, 735-800.
[12] Fitzgerald, J.W. Marine aerosols: a review. *Atmos. Environ*. **1991**, *25A*, 533-546.
[13] Textor, C.; Schulz, M.; Guibert, S.; Kinne, S.; Balkanski,Y.; Bauer, S.; Berntsen,T.; Berglen, T.; Boucher, O.; Chin, M.; Dentener, F.; Diehl, T.; Easter, R.; Feichter, H.; Fillmore, D.; Ghan, S.; Ginoux, P.; Gong, S.; Grini, A.; Hendricks, J.; Horowitz, L.; Huang, P.; Isaksen, I.; Iversen, I.; Kloster, S.; Koch, D.; Kirkevåg, A.; Kristjansson, J.E.; Krol, M.; Lauer, A.; Lamarque, J.F.; Liu, X.; Montanaro, V.; Myhre, G.; Penner, J.; Pitari, G.; Reddy, S.; Seland, Ø.; Stier, P.; Takemura,T. and Tie, X. *Atmos. Chem. Phys.* **2006**, *6*, 1777-1813.
[14] Monahan, E.C, Muircheartaigh, I.O. Optimal Power-Law Description of Oceanic Whitecap coverage Dependence on Wind Speed. *Journal of Physical Oceanography*. **1980**, *10*, 2094-2099.

[15] De Leeuw, G., Neele, F.P., Hill, M., Smith, M.H., Vignati, E. Production of sea spray aerosol in the surf zone, *J. Geophys. Res.*, **2000**, *105*, 29397-29409.
[16] Osterroh, C. Extraction of dissolved fatty acids from sea water. *Fresenius J. Anal. Chem.* **1993,** *345*, 773-779.
[17] Ellison, G.B.; Tuck, A.F.; Vaida, V. Atmospheric processing of organic aerosols. *J. Geophys. Res.* **1999,** *104*, 11633-11641.
[18] Middlebrook, A.M.; Murphy, D.M.; Thomson, D.S. Observations of organic material in individual marine particles at Cape Grim during the First Aerosol Characterization Experiment (ACE 1). *J. Geophys. Res.* **1998**, *103*, 16475-16483.
[19] O'Dowd, C.D.; Facchini, M.C.; Cavalli, F.; Ceburnis, D.; Mircea, M.; Decesari, S.; Fuzzi, S.; Yoon, Y.J.; Putaud, J-P. Biogenically driven organic contribution to marine aerosol. *Nature.* **2004**, *431*, 676-677.
[20] Xiao, H.S.; Dong, J.; Wang, L.; Zhao, L.; Wang, F.; Zhang, Y. Spatially Resolved Micro-Raman Observation on the Phase Separation of Effloresced Sea Salt Droplets. *Enviro. Sci. Tech.*, **2008**, *42*, 8698-8702.
[21] Buseck, P.R.; Posfai, M. Airborne minerals and related aerosol particles: effects on climate and the environment. *Proc. Natl. Acad. Sci.* **1999**, *96*, 3372-3379.
[22] Moffet, R.C.; Prather, K.A. In-situ measurements of the mixing state and optical properties of soot with implications for radiative forcing estimates. *Proc. Natl. Acad. Sci.* **2009**, *106,* 11872-11877.
[23] Kwamena, N.-O.A.; Buajarern, J.; Reid, J.P. Equilibrium Morphology of Mixed Organic/Inorganic/Aqueous Aerosol Droplets: Investigating the Effect of Relative Humidity and Surfactants. *J. Phys. Chem. A*. **2010**, *114*, 5787-5795.
[24] Ciobanu, V.G.; Marcolli,C.; Krieger, U.K.; Weers, U.; Peter, T. Liquid-liquid phase separation in mixed organic/inorganic aerosol particles. *J. Phys. Chem. A.* **2009**, *113*, 10966-10978.
[25] Freedman. M.A.; Hasenkopf, C.A.; Beaver, M.R.; Tolbert, M. Optical Properties of Internally Mixed Aerosol Particles Composed of Dicarboxylic Acids and Ammonium Sulfate. *J. Phys. Chem. A*, **2009**, *113*, 13584-13592.
[26] Song, M.; Marcolli, C.; Kireger, U.K.; Zuend, A.; Peter, T. Liquid-liquid phase separation and morphology of internally mixed dicarboxylic acids/ammonium sulfate/water particles. *Atmos. Chem. Phys.*, **2012**, *12*, 2691-2712.
[27] Kester, D.R.; Ducdall, I.W.; Conners, D.M.; Pytkowicz, R.M. Preparation of Artificial Seawater. *Limnol. Oceanog.* **1967**, *12*, 176-179.
[28] Ghorai, S.; Tivanski, A.V. Hygroscopic behavior of individual submicrometer particles studied by X-ray Spectromicroscopy. *Anal. Chem.* **2010**, *82*, 9289-9298.
[29] Williams, D.B.; Carter, C.B. The Instrument. *Transmission Electron Microscopy: A Textbook for Materials Science*, 2nd Edition; Springer: New York, 2009; pp 151-153.
[30] Haynes, W.M. *CRC Handbook of chemistry and Physics,* 93rd ed. online; 2012; Lattice Constants for Cubic Crystals.
[31] Matijevic, E.; Pethica, B.A. The properties of ionized monolayers, Part 1. Sodium dodecyl sulfate at the air/water interface. *Trans. Faraday Soc.* **1958,** *54,* 1383-1389.
[32] McNeill, V.F.; Patterson, J.; Wolfe, G.M.; Thorton, J.A. The effect of varying levels of surfactant on the reactive uptake of N_2O_5 aqueous aerosol. *Atmos. Chem. Phys.* **2006**, *6*, 1635-1644.

[33] Beaver, M.R.; Freedman, M.A.; Hasenkopf, C.A., Tolbert, M.A. Cooling Enhancement of Aerosol Particles Due to Surfactant Precipitation. *J. Phys. Chem. A*, **2010**, *114*, 7070-7076.
[34] Zelenyuk, A.; Imre, A.; Cuadra-Rodriguez, L.A.; Ellison, B. Measurements and interpretation of the effect of a soluble organic surfactant on the density, shape and water uptake of hygroscopic particles. *Journal of Aerosol Science.* **2007**, *38*, 903-923.
[35] Finlayson-Pitts, B. J.; Pitts, J.N., *Chemistry of the Upper and Lower atmosphere;* Academic Press: New York, 2000; 407-411.
[36] Branda, M.; Di Valentin, C.; Pacchioni, G. NO and NO_2 Adsorption on Terrace, Step, and Corner Sites of the BaO Surface from DFT Calculations. *J. Phys. Chem. B.* **2004,** *108* (15), 4752-4758.
[37] Nygren, M.A.; Petterson, L. Comparing ab initio computed energetics with thermal experiments in surface science: CO/MgO(001). *J. Chem. Phys.* **1996,** *105*, 9339.
[38] Cosman, L.M.; Knopf, D.A.; Bertram, A.K. N_2O_5 reactive uptake on aqueous sulfuric acid solutions coated with branched and straight chain insoluble organic surfactants. *J.Phys.Chem. A.* **2007**, *112*, 2386-2396.
[39] Park, S.C.; Burden, D.K.; Nathanson, G.M. The Inhibition of N_2O_5 hydrolysis in sulfuric acid by 1-butanol and 1-hexanol surfactant coatings. *J. Phys. Chem. A.* **2007**, *111(15)*, 2921-2929.
[40] Cosman, L.M.; Bertram, A.K. Reactive uptake of N_2O_5 on aqueous solutions coated with 1-component and 2-component monolayers. *J.Phys.Chem. A.* **2008**, *112*, 4625-4635.
[41] Bohren, C.F.; Huffman, D.R. Introduction. *Absorption and Scattering of Light by Small Particles,* Wiley-VCH: Weinheim, 2004, pp 4-8.
[42] Liou, K.N. Influence of Cirrus Clouds on Weather and Climate Processes: A Global Perspective. *Mon. Weather. Rev.* **1986**, *114*, 1167-1199.
[43] Wylie, D.P.; Menzel, W.P.; Woolf, H.M.; Strabala, K.I. Four Years of Global Cirrus Cloud Statistics using HIRS. *J. Clim.* **1994**, *7*, 1972-1986.
[44] Lee, S. S.; Penner, J. E. Aerosol effects on ice clouds: can the traditional concept of aerosol indirect effects be applied to aerosol-cloud interactions in cirrus clouds? *Atmos. Chem. Phys.* **2010**, *10*, 10345-10358.
[45] Twohy, C.H.; Poellot, M.R. Chemical characteristics of ice residual nuclei anvil cirrus clouds: evidence of homogeneous and heterogeneous ice formation. *Atmos. Chem. Phys*., **2005**, *5*, 2289-2297.
[46] Zuberi, B.; Bertram, A.; Koop, T.; Molina, L.; Molina, M. Heterogeneous freezing of aqueous particles induced by crystallized $(NH_4)_2SO_4$, ice, and letovicite. *J. Phys. Chem. A.* **2001**, *105*, 6458-6464.
[47] Cziczo, D.; Abbatt, J. Ice nucleation in NH_4HSO_4, NH_4NO_3, and H_2SO_4 aqueous particles: Implications for cirrus cloud formation. *Geophys. Res. Lett.* **2001**, *28*, 963-966.
[48] Mohler, O.; Stetzer, O.; Schaefers, S.; Linke, C.; Schnaiter, M.; Tiede, R.; Saathoff, H.; Kramer, M.; Mangold, A.; Budz, P.; Zink, P.; Schreiner, J.; Mauersberger, K.; Haag, W.; Karcher, B.; Schurath, U. Experimental investigation of homogeneous freezing of sulphuric acid particles in the aerosol chamber AIDA. *Atmos. Chem. Phys.* **2003**, *3*, 211-223.
[49] Martin, S.T.; Phase Transitions of Aqueous Atmospheric Particles. *Chem. Rev.* **2000**, *100*, 3403-3453.
[50] Fletcher, N.H. Active sites and ice crystal nucleation. *J. Atmos. Sci.* **1969**, *26*, 1266-1271.

[51] Talbot, R.W.; Dibb, J.E.; Loomis, M.B. Influence of vertical transport on free tropospheric aerosols over the central USA in springtime. *Geophys. Res. Let.* **1998**, *25*, 1367-1370.
[52] Chen, Y.; Kreidenweis, S.M.; McInnes, L.M.; Rogers, D.C.; DeMott, P.J. Single particle analyses of ice nucleating aerosols in the upper troposphere and lower stratosphere. *Geophys. Res. Let.* **1998**, *25*, 1391-1394.
[53] Abbatt, J.P.D.; Benz, S.; Cziczo, D.J.; Zanji, Z.; Lohmann, U.; Mohler, O. Solid Ammonium Sulfate Aerosols as Ice Nuclei: A Pathway for Cirrus Cloud Formation. *Science*. **2006**, *313*, 1770.
[54] Thiel, P.A.; Madey, T.E. The interaction of water with solid surfaces: Fundamental Aspects. *Surf. Sci. Reports.* **1987**, *7*, 211-385.
[55] Schlichting, H.; Menzel, D. Techniques for wide range, high resolution and precision, thermal desorption measurements. *Surface Science.* **1993**, *285*, 209-218.
[56] McCash, E.M. Adsorption and Desorption. *Surface Chemistry*, Oxford University Press: New York, 2001; pp 81-84.
[57] Christmann, K; Ertl, G.; Shimizu, H. Model Studies on Bimetallic Cu/Ru Catalysts I. *J. Catal.* **1980**, *61*, 397-411.
[58] Behm, R.J.; Christmann, K.; Ertl, G.; van Hove, M.A. Adsorption of CO on Pd(100). *J. Chem. Phys.* **1980**, *73*, 2984-2993.
[59] Christmann, K. Adosrption of Hydrogen on a Nickel (100) surface. *Z. Naturf.* **1979**, *34a*, 22-29.
[60] Grimm, R.L.; Barrentine, N.M.; Knox, C.J.H.; Hemminger, J.C. D_2O Water Interaction with Mixed Alkane Thiol Monolayers of Tuned Hydrophobic and Hydrophilic Character. *J. Phys. Chem. C Let.* **2008,** *112*, 890-894.
[61] de Jong, A.M.; Niemantsverdriet, J.W. Thermal Desorption Analysis: Comparative Test of Ten Commonly Applied Procedures. *Surf. Sci.* **1990**, *233*, 355-365.
[62] Redhead, P.A. Thermal Desorption of Gases. *Vacuum.* **1962**, *12*, 203-211.
[63] Barrie, P.J. Analysis of temperature programmed desorption (TPD) data for the characterization of catalysts containing a distribution of adsorption sites. *Phys. Chem. Chem. Phys.* **2008,** *10*, 1688-1696.
[64] Sugisaki, M.; Suga, H.; Seki, S. Calorimetric study of the glassy state. IV. Heat capacities of glassy water and cubic ice. *S. Bull. Chem. Soc. Jpn.* **1968**, *41*, 2591-2599.
[65] Smith, R.S.; Huang, C.; Wong, E.K.L.; Kay, B.D. Desorption and crystallization kinetics in nanoscale thin films of amorphous water ice. *Surf. Sci.* **1996**, *367*, L13.
[66] Hallbrucker, A.; Mayer, E.; Johari, G.P. Glass-liquid transition and the enthalpy of devitrification of annealed vapor-deposited amorphous solid water: a comparison with hyperquenched glassy water. *J. Phys. Chem.* **1989**, *93*, 4986.
[67] Lofgren, P.; Ahlstrom, P.; Lausma, J.; Kasemo, B.; Chakarov, D. Crystallization Kinetics of Thin Amorphous Water Films on Surfaces. *Langmuir* **2003**, *19*, 265.
[68] Engquist, I.; Lundstrom, I.; Liedberg, B. Temperature-Programmed Desorption and Infrared Studies of D_2O Ice on Self-Assembled Alkanethiolate Monolayers: Influence of Substrate Wettability. *J. Phys. Chem.* **1995**, *99*, 12257-12267.
[69] Smith, R.S.; Matthiesen, J.; Knox, J.; Kay, B.D. Crystallization Kinetics and Excess Free Energy of H_2O and D_2O Nanoscale Films of Amorphous Solid Water. *J. Phys. Chem. A.* **2011**, *115*, 5908-5917.

[70] Brown, T.L.; LeMay, H.E.; Bursten, B.E.; Murphy, C.J. *Chemistry the Central Science*, 11th Edition; Pearson Prentice Hall: NJ, 2009, pp 1111.
[71] Folsch, S.; Stock, A.; Henzler, M. Two-dimensional water condensation on the NaCl(100) surface. *Surface Science* **1992**, *264*, 65-72
[72] Bruch, L.W.; Glebov, A.; Toennies, J.P.; Weiss, H.J. A helium atom scattering study of water adsorption on the NaCl (100) single crystal surface. *J. Chem. Phys.* **1995**, *103*, 5109.
[73] Peters, S.J.; Ewing, G.E. Water on Salt: An Infrared Study of Adsorbed H_2O on NaCl (100) under Ambient Conditions. *J. Phys. Chem. B* **1997**, *101*, 10880-10886.
[74] Wassermann, B.; Mirbt, S.; Reif, J.; Zink, J.C.; Matthias, E. Clustered water adsorption on the NaCl (100) surface. *J. Chem. Phys.* **98**, *12*, 1993.
[75] Ahmed, A.I.; Perry, S.S.; El-Bjeirami, O. Desorption and Reaction of Water on MgO (100) Studied as a Function of Surface Preparation. *J. Phys. Chem. B.* **2000**, *104*, 3343-3348.
[76] Nuzzo, R.G.; Zegarski, B.R.; Dubois, L.H. Fundamental Studies of the Chemisorption of Organosulfur Compounds on Au(111). Implications of Molecular Self-Assembly on Gold Surfaces. *J. Am. Chem. Soc.* **1987,** *109***, 733-740.**
[77] Petrenko, V.; Whitworth, R. *Physics of Ice*; Oxford University Press: Oxford, 1999.
[78] Johari, G.P.; Hallbrucker, A.; Mayer, E. The dielectric behavior of vapor deposited amorphous solid water and of its crystalline forms. *J. Chem. Phys.* **1991**, *95*, 2955.
[79] Dai, Q.; Hu, J.; Salmeron, M. Adsorption of Water on NaCl (100) Surfaces: Role of Atomic Steps. *J. Phys. Chem. B* **1997**, *101*, 1994-1998.
[80] McNaughton, C.S.; Clarke, A.D.; Kapustin, V.; Shinozuka, Y.; Howell, S.G.; Anderson, B.E.; Winstead, E.; Dibb, J.; Scheuer, E.; Cohen, R.C.; Wooldridge, P.; Perring, A.; Huey, L.G.; Kim, S.; Jimenez, J.L.; Dunlea, E.J.; DeCarlo, P.F.; Wennberg, P.O.; Crouse, J.D.; Weinheimer, A.J.; Flocke, F. Observations of heterogeneous reactions between Asian pollution and mineral dust over the Eastern North Pacific during INTEX-B. *Atmos. Chem. Phys.* **2009**, *9*, 8283-8308.
[81] De Leeuw, N.H.; Parker, S.C. Modeling the Competitive Adsorption of Water and Methanoic Acid on Calcite and Fluorite Surfaces. *Langmuir* **1998**, *14*, 5900-5906.
[82] Kerisit, S.; Parker, S.C.; Harding, J.H. Atomistic simulation of the dissociative adsorption of water on calcite surfaces. *J. Phys. Chem. B* **2003**, *107*, 7676-7682.
[83] Chakarov, D.V.; Osterlund, L.; Kasemo, B. Water Adsorption and Coadsorption with Potassium on Graphite (0001). *Langmuir* **1995,** *11*, 1201.
[84] Chakarov, D.; Kasemo, B. Photoinduced Crystallization of Amorphous Ice Films on Graphite. *Phys. Rev. Lett.* **1998**, *81*, 5181.
[85] Bolina, A.S.; Wolff, A.J.; Brown, W.A. Reflection Absorption Infrared Spectroscopy and Temperature Programmed Desorption Studies of the Adsorption and Desorption of Amorphous and Crystalline Water on a Graphite Surface. *J. Phys. Chem. B.* **2005**, *109*, 16836-16845.
[86] Clemens, A.; Hellberg, L.; Gronbeck, H.; Chakarov, D. Water Desorption from Nanostructured Graphite Surfaces. *Phys. Chem. Chem. Phys.* **2013**, *15*, 20456-20462.
[87] Alpert, P.A.; Aller, J.Y.; Knopft, D.A., Ice Nucleation from aqueous NaCl droplets with and without marine diatoms. *Atmos. Chem. Phys.*, **2011**, *11*, 5539-5555.
[88] Wise, M.E.; Baustian, K.J.; Koop, T.; Freedman, M.A.; Jensen, E.J.; Tolbert, M.A. Depositional ice nucleation onto crystalline hydrated NaCl particles: a new mechanism for ice formation in the troposphere. *Atmos. Chem. Phys.* **2012**, *12*, 1121-1134.
[89] Kanji, Z.A.; Abbatt, J.P.D. Laboratory studies of ice formation via deposition mode nucleation onto mineral dust and n-hexane soot samples. *J. Geophys. Res.* **2006**, *111*, D16204.

[90] Falconer, J.L.; Madix, R.J.; Flash Desorption Activation Energies: DCOOH Decomposition and CO Desorption from Ni(110). *Surf. Sci.* **1975**, *48*, 393-405.
[91] King, D.A. Thermal Desorption from Metal Surfaces: A Review. *Surf. Sci.* **1975,** *47*, 384-402.
[92] Habenschaden, E.; Kuppers, J. Evaluation of Flash Desorption Spectra. *Surf. Sci.* **1984**, *138*, L147-L150.